Physica A 514 (2019) 533–548

Contents lists available at ScienceDirect

Physica A

journal homepage: www.elsevier.com/locate/physa

On the relation between a length cutoff in time-convolutionless mode-coupling theory and a characteristic length at β-relaxation stage in glass-forming materials

Michio Tokuyama [a,*], Takayuki Narumi [b]

[a] Institute of Multidisciplinary Research for Advanced Materials, Tohoku University, Sendai 980-8577, Japan
[b] Graduate School of Sciences and Technology for Innovation, Yamaguchi University, Ube 755-8611, Japan

HIGHLIGHTS

- A characteristic length at β stage in glass-forming materials is proposed.
- A length cutoff in memory function of time-convolutionless mode-coupling equation is found.
- Relation of both lengths to caging at β stage is explored.
- Time-convolutionless mode-coupling equation is solved numerically.

ARTICLE INFO

Article history:
Received 13 August 2018
Available online 26 September 2018

Keywords:
Characteristic length
Critical point
Length cutoff
Supercooled liquids
Time-convolutionless mode-coupling theory

ABSTRACT

A length cutoff b contained in the nonlinear memory function of the time-convolutionless mode-coupling theory (TMCT) equation is obtained by solving the TMCT equation in a manner consistent with the simulation results near the glass transition. A characteristic length ℓ of a supercooled liquid is also introduced at a β-relaxation stage based on the mean-field theory proposed by Tokuyama independently and is shown to describe a displacement of a particle in a cage. Then, both lengths are shown to satisfy the inequality $\ell \geq b \geq b_c$ in a supercooled state within an original TMCT equation, where b_c is a critical cutoff obtained independently by solving the Lambert W-function at the critical point. Their control parameter dependence is also explored from a unified point of view. Thus, both lengths are shown to characterize the same caging mechanism at β stage in a supercooled liquid.

1. Introduction

For past few decades, a large number of theoretical attempts has been made to understand the mechanism of the glass transition in various glass-forming materials [1–10]. A well-known theory of this kind is the mode-coupling theory (MCT) [1,2], which was the origin of all later works on the glass transition. Although some of works have been partially successful in specific problems, there does not exist a systematic theory yet which enables us not only to describe the dynamics of supercooled liquids but also to clarify the mechanism of the glass transition from a unifying viewpoint.

* Corresponding author.
E-mail address: tokuyama@tagen.tohoku.ac.jp (M. Tokuyama).

https://doi.org/10.1016/j.physa.2018.09.101
0378-4371/

The principal purpose of the present paper is to propose a statistical–mechanical method of finding a characteristic length ℓ and a length cutoff b contained in the nonlinear memory function consistently at a β-relaxation stage in equilibrium glass-forming liquids. Depending on a space–time scale, there exist different characteristic stages in macroscopic systems. A well-known example of this kind is seen in dilute gases. There are three stages. The first is an initial characteristic stage [N] where the position vector $\boldsymbol{X}_j(t)$ and the momentum $\boldsymbol{P}_j(t)$ of jth particle at time t obey the Newton equation. The second is a kinetic stage [K] where the characteristic length is given by a mean-free path ℓ_f. By setting a cutoff b as $\ell_f \geq b$ in the relevant variables, the Boltzmann equation is thus derived from the Newton equation consistently in the low-density limit. The last is a hydrodynamic stage [H] where there is no characteristic length. By setting b as $b \gg \ell_f$ in the hydrodynamic variables, the hydrodynamic equations are then derived from the Newton equation or from the Boltzmann equation, up to lowest order in $\nabla(\sim O(b^{-1}))$. In the dynamics of equilibrium glass-forming liquids, therefore, there exists three characteristic time stages (see Fig. 1); an initial stage [N] for a short time where the velocity of a particle is given by an average thermal velocity and the ballistic motion dominates the system, a kinetic stage [K] for an intermediate time which consists of two stage, a β-relaxation stage where the caging plays an important role and a α-relaxation stage where the dynamic heterogeneity [11–27] plays an important role, and a hydrodynamic stage [H] for a long time where the diffusion process dominates the system. In the present paper, we focus only on the dynamics at the β-relaxation stage. Then, we find the two lengths b and ℓ independently based on two different theories in three different equilibrium states, [Gas] a gas state, [L] a liquid state, and [S] a supercooled state. The first theory is the time-convolutionless mode-coupling theory (TMCT) [28–31] to find the cutoff b. The other is the mean-field theory (MFT) [32–35] to introduce the length ℓ. Thus, it is explored how both lengths ℓ and b are physically related to each other at a β-relaxation stage in supercooled liquids.

We begin in Section 2 by reviewing TMCT briefly. In order to study the dynamics of glass-forming liquids near the glass transition, Tokuyama has recently proposed TMCT and then derived the TMCT equation from first principles [28–31]. Thus, it has been shown that similarly to MCT, an ergodic to nonergodic transition also occurs in TMCT and also that all the mathematical analyses employed in MCT are directly applicable to TMCT. Hence the next problem left is just how to solve the TMCT equation numerically in a manner consistent with the simulation results or the experimental data. However, we now briefly explain what makes it difficult. Let λ denote a control parameter, such as a volume fraction ϕ and an inverse temperature $1/T$. We take a scaled intermediate scattering function $f_\alpha(q, t)$ to describe the relevant process of interest whose characteristic length is supposed to be ℓ, where the magnitude q of the wave vector $\boldsymbol{q}$ is set as $0 < q \leq b^{-1}$. In general, b is set as $b \leq \ell$. Here $\alpha = c$ stands for a collective part and $\alpha = s$ for a self-part. Then, TMCT provides two types of basic equations. One is a closed nonlinear second-order differential equation (I) for $f_\alpha(q, t)$, which contains the unknown cutoff b through the nonlinear memory function. As λ increases, Eq. (I) ensures that there exists a non-zero solution $f_\alpha(q)$ for long times above the critical point λ_c, at which an ergodic to nonergodic transition occurs. Hence the other is a closed nonlinear equation (or the so-called Lambert W-function) (II) for the non-ergodicity parameter $f_\alpha(q)$, which is derived from Eq. (I) in the long-time limit. This equation enables us to determine a critical point λ_c. In both equations the nonlinear memory functions contain a static structure factor $S(k)$ and depend on b through the relation $0 < k \leq b^{-1}$. If the static structure factor is given, therefore, one can solve Eq. (II) numerically and find a critical cutoff b_c at $\lambda = \lambda_c$. In fact, this has been done by employing the Percus–Yevick (PY) static structure factor [36] for monodisperse hard-sphere systems [37,38]. When $\lambda < \lambda_c$, one has to solve Eq. (I) under an appropriate value of b, which must satisfy the inequality $b(\lambda) \geq b_c$. Since the value of $b(\lambda)$ is in general unknown, however, this makes difficult to solve it even numerically. On the other hand, b_c can be found independently of b under the fact that the diffusion coefficient becomes zero at $\lambda = \lambda_c$. Hence this fact may give us an important hint to find a reasonable value of $b(\lambda)$ [31]. This will be discussed in details later. Finally, we review MFT briefly. Since Eq. (I) does not contain ℓ, it is reasonable to find it independently in a phenomenological manner based on MFT. Then, one can find the characteristic length ℓ at a β-relaxation stage in a supercooled state in addition to a gas state and a liquid state. We also discuss the universality in the dynamics of glass-forming materials, in which the dynamics in different systems coincides with each other if the scaled diffusion coefficient in different systems has the same value. Thus, it is shown that this universality enables us to use the PY static structure factor even for polydisperse hard-sphere systems.

In Section 3, we discuss the characteristic length ℓ at β stage. As a simple example of glass-forming materials, we first take the hard-sphere fluids with size polydispersities. By using the simulation results on those systems, we find the volume fraction ϕ dependence of ℓ in both states [Gas] and [L]. Then, we show that the lengths in both states are characteristic lengths related to the mean-free path ($L_f \sim \phi^{-1}$) and the inter-particle distance ($L_l \sim \phi^{-1/3}$), respectively. In a supercooled state [S], ℓ is shown to obey a power law $\ell \sim \tilde{D}(\phi/\phi_c)^{\mu/2}$, where a scaled diffusion coefficient $\tilde{D}(x)$ is a singular function of x and μ is an exponent to be determined. Hence it is also expected to be a characteristic length, describing a displacement in a cage, which is mostly formed by surrounding particles at a β-relaxation stage. Secondly, we also investigate the length ℓ in two types of glass-forming materials, fragile liquids and strong liquids, and then show that the same power laws as those obtained in hard spheres hold even in their systems, except that ϕ is now replaced by an inverse temperature $1/T$.

In Section 4, in order to obtain the length cutoff $b(\lambda)$ numerically, we choose the hard-sphere fluids as a simple example since the static structure factor for monodisperse hard-sphere systems is given analytically by the PY model [36]. Then, we solve the TMCT equation numerically in a manner consistent with the simulation results on hard spheres and find the length cutoff $b(\phi)$. This is done independently of $\ell(\phi)$. Thus, we check whether $b(\phi)$ satisfies the same power law as that of $\ell(\phi)$ or not and then explore how $b(\phi)$ relates physically to $\ell(\phi)$ at β-relaxation stage in a supercooled state. We conclude in Section 5 with a summary together with the prediction based on the present approach that the four-point dynamic correlation length $\xi_4(\lambda)$ for dynamic heterogeneity at α stage in [S] is inversely proportional to the length $\ell(\lambda)$ at β stage, leading to $\xi_4(\lambda) \propto \ell(\lambda)^{-1} \sim \tilde{D}^{-\mu/2}$.

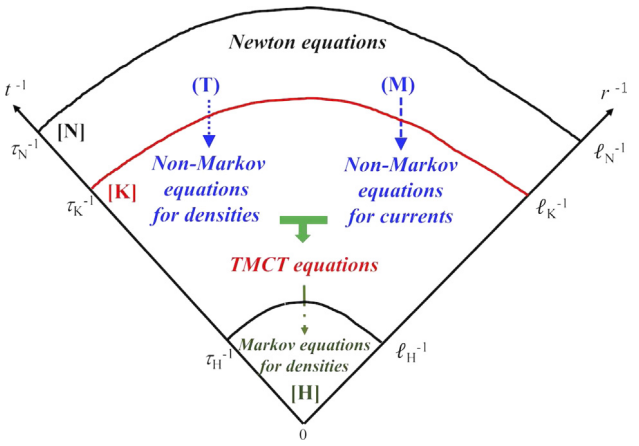

Fig. 1. (Color online) Classification of the basic equations discussed in the present paper into three stages, [N], [K], and [H], depending on a space (r)-time (t) scale, where ℓ_i and τ_i indicate the relevant length and time of interest, respectively.

2. Basic equations

In the present section, we summarize and discuss the basic equations and concepts, which are used in the present paper.

2.1. TMCT equation

In this subsection, we first explain the theoretical background of TMCT and then briefly review the macroscopic equations in the equilibrium molecular systems which are derived from first principles by using a new formulation based on TMCT [28–31]. The outline of TMCT is as follows. As is shown in Fig. 1, depending on a space–time scale, the basic equations in [K] and [H] can be formally derived from the Newton (or Heisenberg) equations in a stage [N]. In a kinetic stage [K], the relevant variables are given by the current densities and the number densities. A generalized linear non-Markov Langevin equation for the current density is derived from the Heisenberg equation by using the Mori projection-operator method [39] (see a dashed arrow (M) in Fig. 1), where the memory term is convolution in time and is written in terms of correlation function of the fluctuating force. A linear non-Markov stochastic diffusion equation for the number density is also derived from the Heisenberg equation by employing the Tokuyama–Mori projection-operator method [40,41] (see a dotted arrow (T) in Fig. 1), where the memory term is convolutionless in time and is written in terms of correlation function of the fluctuating current. Those coupled equations are then used to find a closed nonlinear non-Markov second-order differential equation for the average number density (see a bold arrow in Fig. 1). This is a TMCT equation not only to describe the dynamics of supercooled liquids but also to find a critical point at which an ergodic to non-ergodic transition occurs. In a hydrodynamic stage [H], the Markov diffusion equation for the number density is derived (see a dot-dashed arrow in Fig. 1). Thus, it is shown that the closed nonlinear equation can describe the dynamics of equilibrium glass-forming liquids from an initial stage to a diffusion stage. Here we note that in MCT [1,2] the Mori projection-operator method has been used to obtain the basic equations for both relevant variables. As discussed in the previous papers [28,31], however, it is important to employ two types of projection-operator methods to derive the basic equations for different relevant variables. In fact, it is indispensable to use the time-convolutionless formalism for the number density to recover the cumulant expansion proposed by Kubo [42]. Thus, TMCT enables us to calculate each cumulant-expansion term, such as a mean-square displacement $M_2(t)$ and a non-Gaussian parameter $\alpha_2(t)(=3M_4(t)/5M_2(t)^2-1)$ [43], consistently from first principles, where $M_{2n}(t)=\langle|\boldsymbol{X}_j(t)-\boldsymbol{X}_j(0)|^{2n}\rangle$, the brackets being the average over an equilibrium ensemble.

We now briefly review the TMCT equation in stage [K]. We consider the three-dimensional equilibrium glass-forming system, which consists of N particles with mass m and diameter σ in the total volume V at temperature T. The scaled intermediate scattering function $f_\alpha(q,t)$ is then given by

$$f_\alpha(q,t)=\langle\rho_\alpha(\boldsymbol{q},t)\rho_\alpha(\boldsymbol{q},0)^*\rangle/S_\alpha(q) \tag{1}$$

with the collective density fluctuation

$$\rho_c(\boldsymbol{q},t)=\frac{1}{N^{1/2}}\left[\sum_{j=1}^{N}\rho_s(\boldsymbol{q},t)-N\delta_{\boldsymbol{q},0}\right], \tag{2}$$

and the self-density fluctuation

$$\rho_s(\boldsymbol{q},t)=e^{i\boldsymbol{q}\cdot\boldsymbol{X}_j(t)}, \tag{3}$$

where $\langle \rho_s(\boldsymbol{q}, t)\rangle = \delta_{\boldsymbol{q},0}$ and $\langle \rho_c(\boldsymbol{q}, t)\rangle = 0$, and $q = |\boldsymbol{q}|$. Here $S_c(q) = S(q)$ and $S_s(q) = 1$, where $S(q)(= \langle|\rho_c(\boldsymbol{q}, 0)|^2\rangle)$. Since the density fluctuations $\rho_\alpha(\boldsymbol{q}, t)$ are macroscopic physical quantities, we set $0 < q \leq b^{-1}$. As suggested in the previous paper [31], the cutoff b should be in general fixed so that the numerical solutions of TMCT equation coincide with the simulation results or the experimental data. This will be discussed in details later.

As shown in the previous paper [31], the coupled equations for the scattering function $f_\alpha(\boldsymbol{q}, t)$ and the current–current correlation function $\psi_\alpha(\boldsymbol{q}, t)$ are obtained in stage [K] as

$$\frac{\partial}{\partial t} f_\alpha(q, t) = -q^2 D_\alpha(q, t) f_\alpha(q, t), \tag{4}$$

$$\frac{\partial}{\partial t}\psi_\alpha(q, t) = -\gamma\psi_\alpha(q, t) - \int_0^t \Delta\varphi_\alpha(q, t-s)\frac{f_\alpha(q, s)}{f_\alpha(q, t)}\psi_\alpha(q, s)ds \tag{5}$$

with the q- and t-dependent diffusion coefficient

$$D_\alpha(q, t) = \int_0^t \psi_\alpha(q, s)ds, \tag{6}$$

and the nonlinear memory function

$$\Delta\varphi_\alpha(q, t) = \frac{\rho v_{th}^2}{2^{n_\alpha}} \int_< \frac{d\boldsymbol{k}}{(2\pi)^3} v_\alpha(\boldsymbol{q}, \boldsymbol{k})^2 S(k) S_\alpha(|\boldsymbol{q} - \boldsymbol{k}|) f_c(k, t) f_\alpha(|\boldsymbol{q} - \boldsymbol{k}|, t), \tag{7}$$

where γ is a damping constant to be determined, $n_c = 1$, $n_s = 0$, $\rho = N/V$, and $v_{th}(= (k_B T/m)^{1/2})$ an average thermal velocity. Here $\int_<$ denotes the sum over wave vectors $\boldsymbol{k}$ whose magnitudes are smaller than a cutoff b^{-1}. The vertex amplitude $v_\alpha(\boldsymbol{q}, \boldsymbol{k})$ is given by

$$v_\alpha(\boldsymbol{q}, \boldsymbol{k}) = \hat{\boldsymbol{q}} \cdot \boldsymbol{k} c(k) + n_\alpha \hat{\boldsymbol{q}} \cdot (\boldsymbol{q} - \boldsymbol{k}) c(|\boldsymbol{q} - \boldsymbol{k}|), \tag{8}$$

where $\rho c(k) = 1 - 1/S(k)$ and $\hat{\boldsymbol{q}} = \boldsymbol{q}/q$. Here $\gamma(\lambda)$ is a damping constant which is determined by the fitting with the simulation results or the experimental data and depends only on the extensive parameter, such as the volume fraction ϕ [31]. The initial conditions are given by $f_\alpha(q, 0) = 1$ and $\psi_\alpha(q, 0) = v_{th}^2/S_\alpha(q)$.

In order to obtain a single closed equation from the above coupled equations, it is convenient to introduce the cumulant function $K_\alpha(q, t)$ by [28–31]

$$f_\alpha(q, t) = \exp[-K_\alpha(q, t)]. \tag{9}$$

By taking the Laplace transform of Eqs. (4) and (5), one can then obtain the closed nonlinear second-order differential equation for $K_\alpha(q, t)$ as [31]

$$\frac{\partial^2 K_\alpha(q, t)}{\partial t^2} = \frac{q^2 v_{th}^2}{S_\alpha(q)} - \gamma\frac{\partial K_\alpha(q, t)}{\partial t} - \int_0^t ds \int_0^s d\tau \Delta\varphi_\alpha(q, s-\tau)\frac{f_\alpha(q, \tau)}{f_\alpha(q, s)}\frac{\partial^2}{\partial\tau^2}K_\alpha(q, \tau). \tag{10}$$

Eq. (10) is a TMCT equation to describe the dynamics of equilibrium glass-forming liquids. From Eq. (10), one can easily find the asymptotic solutions. In an initial stage for a short time of order $\tau_\gamma(= 1/\gamma)$, one obtains

$$K_\alpha(q, t) \simeq q^2 \frac{v_{th}^2}{\gamma^2 S_\alpha(q)}(\gamma t - 1 + e^{-\gamma t}), \tag{11}$$

which leads to $K_\alpha(q, t) \simeq q^2 v_{th}^2 t^2/2S_\alpha(q)$ for $t \ll \tau_\gamma$. On the other hand, in a diffusion stage [H] for a long time, one also obtains

$$K_\alpha(q, t) \simeq q^2 D_\alpha(q) t \tag{12}$$

with the q-dependent long-time diffusion coefficient

$$D_\alpha(q) = D_\alpha(q, t = \infty) = \frac{v_{th}^2/S_\alpha(q)}{\gamma + \int_0^\infty \Delta\varphi_\alpha(q, s)ds}. \tag{13}$$

As shown in the previous paper [31], Eq. (10) ensures an existence of ergodic to non-ergodic transition at a critical point λ_c, above which the scaled scattering function $f_\alpha(q, t)$ reduces to a non-zero value $f_\alpha(q)$ for long times, the so-called nonergodicity parameter. When $\lambda \geq \lambda_c$, introducing the nonergodicity cumulant $K_\alpha(q)$ by

$$f_\alpha(q) = \exp[-K_\alpha(q)], \tag{14}$$

one can obtain a closed equation for $K_\alpha(q)$

$$K_\alpha(q)\mathcal{F}_\alpha(q) = 1 \tag{15}$$

with the long-time limit of the memory function

$$\mathcal{F}_\alpha(q, f_c, f_\alpha) = \frac{1}{2^{n_\alpha}(2\pi)^3}\int_< d\boldsymbol{k} V_\alpha^{(2)}(q, k, |\boldsymbol{q}-\boldsymbol{k}|) f_c(k) f_\alpha(|\boldsymbol{q}-\boldsymbol{k}|), \tag{16}$$

where the vertex $V_\alpha^{(2)}$ is given by

$$V_\alpha^{(2)}(q, k, |\boldsymbol{q}-\boldsymbol{k}|) = \rho S_\alpha(q) S_c(k) S_\alpha(|\boldsymbol{q}-\boldsymbol{k}|) v_\alpha(\boldsymbol{q}, \boldsymbol{k})^2/q^2. \tag{17}$$

The critical point λ_c is thus determined by solving Eq. (15) numerically. In fact, $K_\alpha(q)$ is considered to be a kind of the Lambert W-function. Hence this mathematically ensures that there exists a critical point. Then, it is shown that at the critical point there exists a maximum critical cutoff b_c, where the nonergodic parameter $f_\alpha(q)$ reduces to 0 at $q = b_c^{-1}$. This means that the value of λ_c does not change even if the cutoff b is set to be $b \le b_c$. The existence of such a maximum value is mainly due to the fact that the static structure factor $S(q)$ reduces to a unity at not so large value of q. Since b is a length cutoff of ℓ, therefore, it is expected to satisfy the inequality $\ell \ge b \ge b_c$ for $\lambda \le \lambda_c$. We also note here from Eq. (13) that at λ_c the diffusion coefficient $D_\alpha(q)$ becomes 0 as $D_\alpha(q) \sim \lim_{t\to\infty}(t\mathcal{F}_\alpha(q))^{-1} = 0$.

In order to discuss the dynamics of glass-forming liquids, one has to solve Eq. (10) numerically by choosing an appropriate value of $b(> b_c)$ for $\lambda < \lambda_c$. The long-time self-diffusion coefficient is usually obtained not only by the simulations but also by experiments. Hence the easiest way to find the cutoff b is to solve Eq. (10) consistently so that the diffusion coefficient coincides with that of the simulation results or that of experimental data. In fact, as shown in Ref. [31], from Eq. (10) one can obtain the following equation for the mean-square displacement $M_2(t)$:

$$M_2(t) = 6\frac{v_{th}^2}{\gamma^2}(\gamma t - 1 + e^{-\gamma t}) - \int_0^t \Gamma_0(t-s) M_2(s) ds \tag{18}$$

with the nonlinear memory term

$$\Gamma_0(t) = \frac{\rho v_{th}^2}{6\pi^2}\int_0^{1/b} dk k^4 c(k)^2 S(k) \int_0^t ds e^{-\gamma(t-s)} f_c(k, s) f_s(k, s). \tag{19}$$

For $t \gg \tau_\gamma$, Eq. (18) then reduces to $M_2(t) \simeq 6D_s^L t$ with the long-time self-diffusion coefficient

$$D_s^L = \frac{v_{th}^2}{\gamma + \frac{\rho v_{th}^2}{6\pi^2}\int_0^{1/b} dk k^4 c(k)^2 S(k) \int_0^\infty ds f_c(k, s) f_s(k, s)}. \tag{20}$$

In Section 4, we show how the cutoff $b(\lambda)$ is found consistently under the condition that the self-diffusion coefficient D_s^L given by Eq. (20) coincides with that obtained from the simulation results. Thus, we explore the physical role of b in the memory function and also check under which circumstance the inequality $\ell \ge b$ holds. Finally, we mention that $D_s^L = 0$ at $\lambda = \lambda_c$. Thus, it turns out that the critical cutoff b_c can be in principle also obtained by solving Eq. (10) under the condition $D_s^L = 0$.

2.2. Mean-field theory

In this subsection, we introduce a mean displacement ℓ and discuss its related mechanism. In order to describe the dynamics of the glass-forming liquids, the following mean-field equation has been proposed for $M_2(t)$ [32,33]:

$$\frac{d}{dt}M_2(t) = 6D_s^L + 6[v_{th}^2 t - D_s^L] e^{-M_2(t)/\ell^2}. \tag{21}$$

Here ℓ is a mean displacement over which a particle can move freely. Eq. (21) is easily solved to give

$$M_2(t) = 6D_s^L t + \ell^2 \ln\left[e^{-6t/\tau_\beta} + \frac{1}{6}\left(\frac{\tau_\beta}{\tau_f}\right)^2\left\{1 - \left(1 + \frac{6t}{\tau_\beta}\right)e^{-6t/\tau_\beta}\right\}\right] \tag{22}$$

with the β-relaxation time for a particle to diffuse over a distance of order ℓ with the diffusion coefficient D_s^L

$$\tau_\beta = \ell^2/D_s^L, \tag{23}$$

where $\tau_f (= \ell/v_{th})$ is a mean-free time for a particle to move over a distance of order ℓ with the velocity v_{th}. From Eq. (22), we have $M_2(t) \simeq 3v_{th}^2 t^2$ for a short time $t \ll \tau_f$, while $M_2(t) \simeq 6D_s^L t$ for a long time $t \gg \tau_\beta$. Hence the intermediate-time region for $\tau_f \le t \le \tau_\beta$ is the so-called β-relaxation stage, where a cage related to ℓ is formed. The numerical value of ℓ can be obtained only by fitting Eq. (22) with the simulation results or the experimental data. As is shown in Fig. 2, however, this fitting works well only in a liquid state [L] but not in a supercooled state [S], where in the β stage the solution does not fit with the simulation results in [S], while it does in [L]. Hence the fitting value ℓ has an ambiguity in [S]. In order to avoid this difficulty, one may separate the mean-field solution into two parts [32,33]; the fast-relaxation part

$$M_2^f(t) = \ell^2 \ln\left[1 + \frac{1}{6}\left(\frac{\tau_\beta}{\tau_f}\right)^2\left\{1 - \left(1 + \frac{6t}{\tau_\beta}\right)e^{-6t/\tau_\beta}\right\}\right], \tag{24}$$

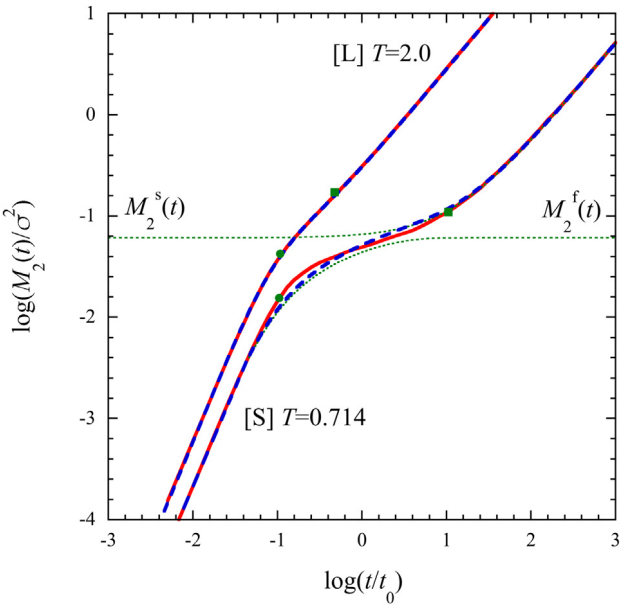

Fig. 2. (Color online) A log–log plot of the scaled mean-square displacement $M_2(t)/\sigma^2$ versus scaled time t/t_0 for the Stillinger–Weber (SW) binary mixtures $A_{80}B_{20}$, where $t_0 = \sigma/v_{th}$. The solid lines indicate the simulation results [44–46] at $T = 2.0$ [L] and 0.714 [S]. The long-dashed lines indicate the mean-field solution given by Eq. (22), where $\ell/\sigma = 0.149$ [L] and 0.09434 [S] and $D_s^L/\sigma v_{th} = 4.682\times10^{-2}$ [L] and 8.438×10^{-4} [S]. The dotted lines indicate the fast- and slow-relaxation parts in [S], where $\ell/\sigma = 0.09089$ and $D_s^L/\sigma v_{th} = 8.438\times10^{-4}$. The symbols (•) indicate the mean-free time τ_f and (□) the β-relaxation time τ_β.

and the slow-relaxation part

$$M_2^s(t) = 6D_s^L t + \ell^2 \ln\left[e^{-6t/\tau_\beta} + \frac{1}{6}\left(\frac{\tau_\beta}{\tau_f}\right)^2\right]. \tag{25}$$

Those solutions lead to the following asymptotic forms:

$$M_2^f(t) \simeq \begin{cases} 3v_{th}^2 t^2, & \text{for } t \ll t_0, \\ \ell^2 \ln[1 + \frac{1}{6}(\frac{\tau_\beta}{\tau_f})^2], & \text{for } t \gg t_0, \end{cases} \tag{26}$$

$$M_2^s(t) \simeq \begin{cases} \ell^2 \ln[1 + \frac{1}{6}(\frac{\tau_\beta}{\tau_f})^2], & \text{for } t \ll t_0, \\ 6D_s^L t, & \text{for } t \gg t_0. \end{cases} \tag{27}$$

Then, the mean displacement ℓ is obtained so that the slow-relaxation part has a better fit with the simulation result in the β-relaxation stage for $\tau_f \le t \le \tau_\beta$. Thus, the reliable value of ℓ can be found consistently. In fact, as is shown in Fig. 2, from the simulation results at $T = 0.714$ one can find $\ell/\sigma = 0.09089$ by using Eq. (25), instead of the direct fitting value 0.09434 obtained by Eq. (22). In the next section, we show that the displacement ℓ in [S] plays a role of a characteristic length to describe a caging in the β stage.

2.3. Universality

We finally discuss the universality in the dynamics of glass-forming materials [32–35]. If the scaled diffusion coefficient $\tilde{D}(= q_m D_s^L/v_{th})$ has the same value even in different systems, the scaled mean-square displacements $q_m^2 M_2(t)$ obtained in the different systems versus scaled time $q_m v_{th} t$ coincide with each other, where q_m is the first peak position of the static structure factor $S(q)$. The simple examples of such a universality are seen in Fig. 3. This is because the universal parameter $\tilde{D}$ is described by a singular function of λ/λ_c. As discussed in Refs. [34,35], the α- and β-relaxation times τ_α and τ_β of the self-diffusion process in [S] are shown to obey the power laws

$$\tau_\alpha \propto \tilde{D}^{-(1+\mu)}, \quad \tau_\beta \propto \tilde{D}^{-(1-\mu)}, \tag{28}$$

where the exponent μ is given by $\mu \simeq 2/10$ for fragile liquids and 2/11 for strong liquids. From Eqs. (23) and (28), the scaled length ℓq_m at β stage then obeys the universal function

$$\ell q_m = L(\lambda/\lambda_c) \propto \tilde{D}^{\mu/2}. \tag{29}$$

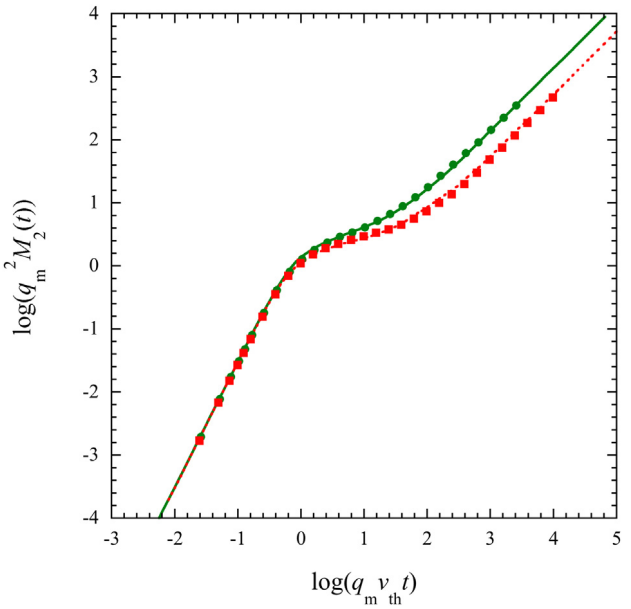

Fig. 3. (Color online) A log–log plot of the scaled mean-square displacement $q_m^2 M_2(t)$ versus scaled time $q_m v_{th} t$ for different systems. The solid line indicates the simulation results on the SW binary mixtures $A_{80}B_{20}$ at $T = 0.833$ [44–46] and the dotted line on the Lennard-Jones (LJ) binary mixtures $A_{80}B_{20}$ at $T = 0.588$ [47,48], where $q_m\sigma = 7.25$. The symbols indicate the simulation results on Al_2O_3 [45,46]; (•) at $T = 3100$ (K) and (□) at $T = 2700$ (K), where $q_m = 2.7$ (Å).

Table 1
ϕ_c, ϕ_s, and ϕ_l for different values of δ.

δ	ϕ_l	ϕ_s	ϕ_g	ϕ_c
0.00	0.4000	0.5315	0.5799[a]	0.5820
0.06	0.4017	0.5338	0.5824[a]	0.5845
0.15	0.4068	0.5405	0.5898	0.5919

[a]Indicates the expected value from $\phi_g(\delta = 0.15)$.

By using Eqs. (28) and (29), one can also predict that the length at α stage must be proportional to ℓ^{-1} and satisfies the relation

$$\tau_\alpha \propto \ell^{-2}/\tilde{D}. \tag{30}$$

This will be briefly discussed in Section 5 together with the simulation results [21–26] obtained for the coherence length at α stage. Finally, we note that the universal functions $\tilde{D}(x)$ and $L(x)$ depend not only on types of control parameters, an intensive parameter such as inverse temperature $1/T$ and an extensive parameter such as volume fraction ϕ but also on types of liquids, fragile liquids and strong liquids. In the next section, we show the examples of $L(x)$ in different systems.

3. A characteristic length

In this section, we discuss how the mean displacement ℓ obtained by fitting Eq. (25) with various simulation results is related to a well-known characteristic length and then show that ℓ obeys the universal function.

3.1. Hard-sphere fluids

The molecular-dynamics (MD) simulations have been performed on hard spheres with radius a_i and mass m_i ($i = 1, \ldots, N$) in a cubic box of volume V at a constant temperature T [49–52]. The distribution of radii is assumed to obey a Gaussian distribution with the standard deviation δ divided by the average radius a, where m_i is proportional to a_i^3. Then, the volume fraction $\phi(\delta)$ is given by $\phi(\delta) = \phi(0)(1 + 3\delta^2)$, where $\phi(0) = 4\pi a^3\rho/3$. The long-time self-diffusion coefficient $D_s^L(\phi, \delta)$ obtained by the MD simulations are then shown to obey the following power law within error:

$$\frac{D_s^L(\phi, \delta)}{a v_0} = \left(1 - \frac{\phi(\delta)}{\phi_c(\delta)}\right)^2, \tag{31}$$

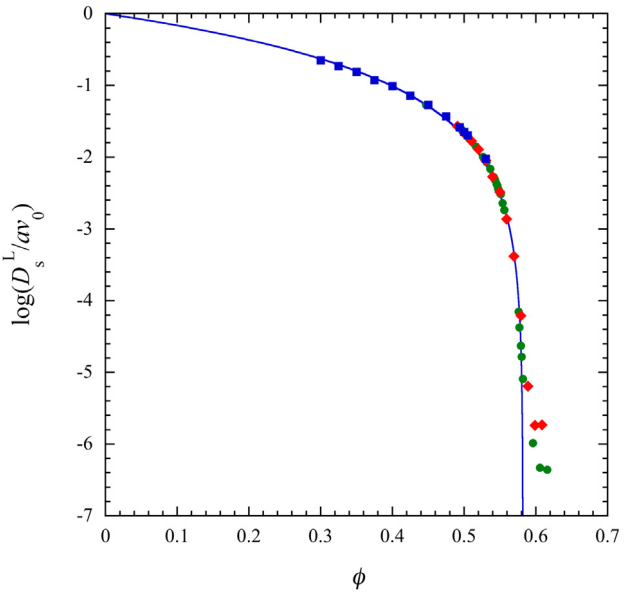

Fig. 4. (Color online) A log plot of the self-diffusion coefficient D_s^L/av_0 versus volume fraction $\phi(0)$. The symbols (□), (○), and (◇) indicate the simulation results at $\delta = 0.0$, 0.06, and 0.15, respectively, where the volume fraction $\phi(\delta)$ is shifted to $\phi(0)$ by using Eq. (32). The solid line indicates the power law given by Eq. (31) at $\delta = 0$.

where $a = \sigma/2$ and $v_0 = \sqrt{3}v_{th}$. From a viewpoint of universality, therefore, the following relation is found:

$$\frac{\phi(\delta)}{\phi_c(\delta)} = \frac{\phi(\delta')}{\phi_c(\delta')}, \tag{32}$$

where the critical volume fraction $\phi_c(\delta)$ is listed in Table 1 for three different values $\delta = 0.00$, 0.06, and 0.15. By using such a relation, it is thus shown in Fig. 4 that all the simulation results obtained for different values of δ are collapsed into a single power law given by Eq. (31). The length ℓ is also obtained by the best fitting of Eq. (25) with the simulation results in the β-relaxation stage for $\tau_f \le t \le \tau_\beta$ (see Fig. 5). We next discuss two cases for $\delta = 0.00$ and 0.15, separately.

3.1.1. Monodisperse case ($\delta = 0$)

In Fig. 6, the scaled displacement ℓ/σ is plotted versus ϕ. As ϕ increases, ℓ drastically decreases up to $\phi = \phi_l(0)$, where $\phi_l(0)$ is a liquid point whose value is listed in Table 1. This region is considered to be a gas state [Gas]. In fact, the mean-free path L_f for the Maxwell distribution of velocity is given by $L_f(\phi) = 1/(2^{1/2}\pi a^2\rho) = 2^{1/2}\sigma/(3\phi)$. Hence the displacement $\ell_f(\phi, 0)$ over which the particle can move freely is given by

$$\ell_f(\phi(0)) = L_f - \sigma = \left(\frac{2^{1/2}}{3}\phi^{-1} - 1\right)\sigma. \tag{33}$$

Then, the simulation results are shown to be well described by ℓ_f up to ϕ_l within error. For $\phi_l(0) \le \phi \le \phi_s(0)$, ℓ gradually decrease, where $\phi_s(0)$ is a supercooled point whose value is listed in Table 1. This region must be a liquid state [L]. The average inter-particle distance L_l is given by $L_l(\phi) = a/\phi^{1/3}$. Hence the displacement $\ell_l(\phi, 0)$ is given by

$$\ell_l(\phi(0)) = L_l - a = \left(\phi^{-1/3} - 1\right)\frac{\sigma}{2}. \tag{34}$$

The simulation results are also shown to be well described by ℓ_l up to ϕ_s within error. For $\phi > \phi_s(0)$, the simulation results start to decrease drastically, leading to the crystallization. Thus, it turns out that in monodisperse hard spheres, the gas line ℓ_f is related to the mean-free path L_f and the liquid line ℓ_l to the inter-particle distance L_l. Hence the mean displacement ℓ is considered to be related to a characteristic length to describe a β-relaxation process.

3.1.2. Polydisperse case ($\delta \neq 0$)

In order to find a characteristic length in a supercooled state [S], we now discuss the polydisperse case ($\delta \neq 0$). Similarly to the monodisperse case, the displacement $\ell(\phi, \delta)$ is obtained from the fitting with the simulation results at $\delta = 0.06$ and 0.15 consistently. In Fig. 7, the fitting results for $\ell(\phi(0.15))$ are shown versus ϕ. In both states [Gas] and [L], the fitting results are shown to be described well by the following universal functions:

$$\ell_f(\phi(\delta)) = \left[\frac{2^{1/2}}{3}\left(\frac{\phi_c(0)\phi(\delta)}{\phi_c(\delta)}\right)^{-1} - 1\right]\sigma, \tag{35}$$

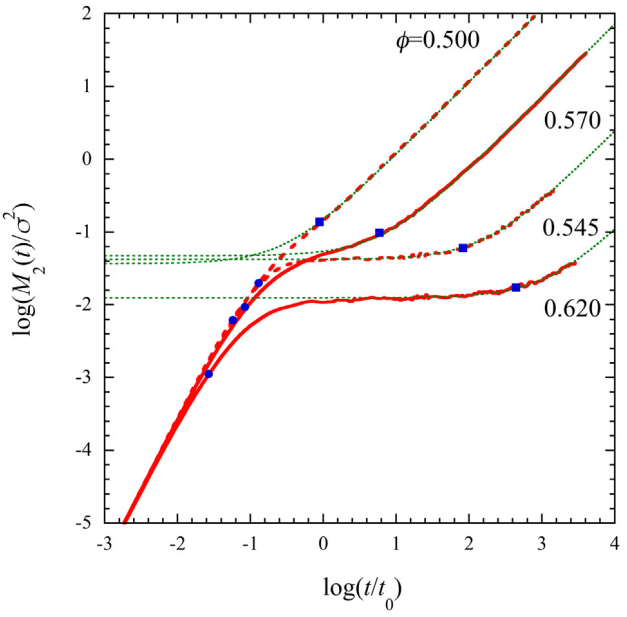

Fig. 5. (Color online) A log–log plot of the scaled mean-square displacement $M_2(t)/\sigma^2$ versus scaled time t/t_0 for hard-sphere fluids. The dashed lines indicate the simulation results at $\delta = 0.0$ for $\phi = 0.500$ [L] and 0.545 [C] and the solid lines the simulation results at $\delta = 0.15$ for $\phi = 0.570$ [S] and 0.620 [G]. The dotted lines indicate the slow-relaxation part given Eq. (25). The details are the same as in Fig. 2.

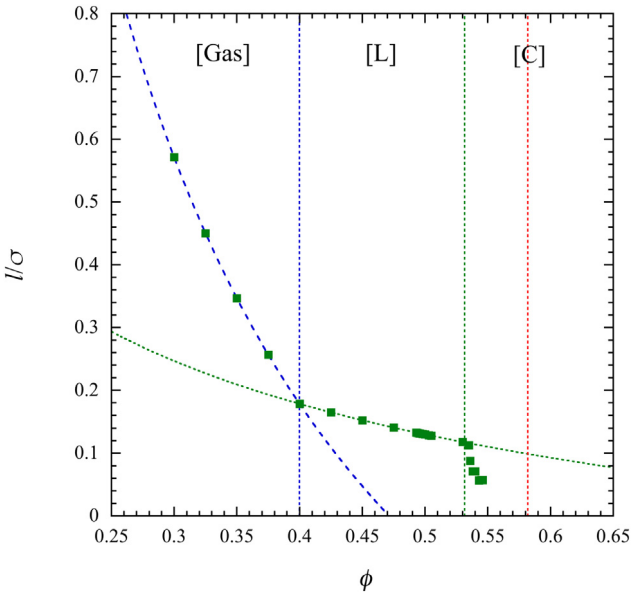

Fig. 6. (Color online) A mean-displacement ℓ/σ versus ϕ for hard-sphere fluids at $\delta = 0$. The symbols (□) indicate the length ℓ obtained from the simulation results. The dashed line indicates the gas line ℓ_f given by Eq. (33) and the dotted line the liquid line ℓ_l given by Eq. (34). The vertical dotted lines indicate ϕ_l, ϕ_s, and ϕ_c from left to right, respectively. [C] stands for a crystal state.

$$\ell_l(\phi(\delta)) = \left[\left(\frac{\phi_c(0)\phi(\delta)}{\phi_c(\delta)}\right)^{-1/3} - 1\right]\frac{\sigma}{2}, \tag{36}$$

where Eq. (32) has been used to extend the lines $\ell_f(\phi(0))$ and $\ell_l(\phi(0))$ to the polydisperse cases. After the liquid state [L], the supercooled state [S] appears for $\phi_s(\delta) \le \phi \le \phi_g(\delta)$, where $\phi_g(\delta)(< \phi_c(\delta))$ is the glass transition volume fraction whose value is listed in Table 1. From Eq. (29), we just assume the simple form for the supercooled line ℓ_s as $1/(\ell_s q_m) = A[B\tilde{D}^{-\mu/2} - 1]$, where the prefactors A and B are found from the fitting with the simulation results in [S] at $\delta = 0.06$ and 0.15. Then, we find

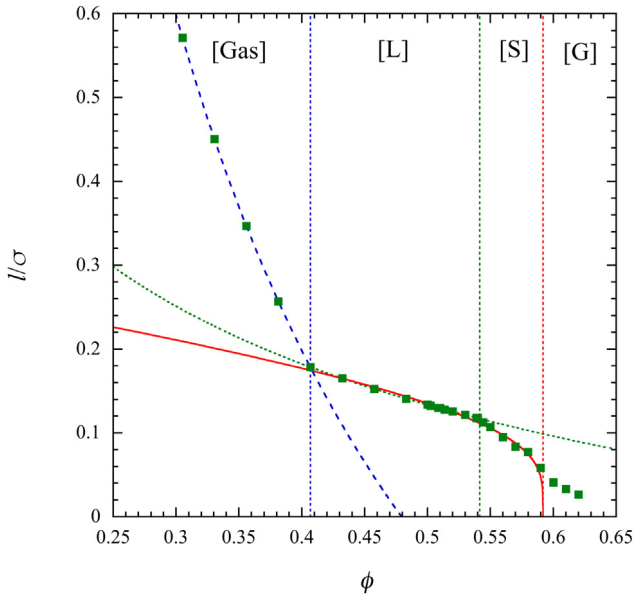

Fig. 7. (Color online) A mean-displacement ℓ/σ versus ϕ for hard-sphere fluids at $\delta = 0.15$. The symbols (□) indicate the length ℓ obtained from the simulation results. The dashed line indicates the gas line given by Eq. (35), the dotted line the liquid line given by Eq. (36), and the solid line the supercooled line given by Eq. (37). [G] stands for a glass state. The details are the same as in Fig. 6.

Table 2
Prefactors A_i and B_i for two types of molecular systems.

State	Prefactor	Fragile liquids	Strong liquids
Liquid state	A_l	0.2757	0.1932
	B_l	3.4159	2.9420
Supercooled state	A_s	0.1874	1.3526
	B_s	5.2279	1.7275

$A \simeq 0.4924$ and $B \simeq 2.6312$. Thus, we obtain

$$\ell_s(\phi(\delta))q_m(\phi(\delta)) = \frac{1}{A[B\tilde{D}(\phi(\delta))^{-\mu/2} - 1]}. \tag{37}$$

Near the critical point, use of Eqs. (31) and (37) then leads to $\ell_s(\phi(\delta)) \propto \tilde{D}^{\mu/2} \propto (1-\phi(\delta)/\phi_c(\delta))^{0.2}$. For $\phi > \phi_g$ the simulation results start to deviate from the supercooled line $\ell_s(\phi(\delta))$. This deviation is corresponding to the fact that the self-diffusion coefficient D_s^L of the simulation results start to deviate from Eq. (31) at ϕ_g (see Fig. 4).

3.2. Two types of glass-forming materials

In this subsection, we discuss the displacement ℓ obtained by the molecular-dynamics simulations performed on two types of glass-forming materials, fragile liquids and strong liquids, separately, in both of which the control parameter is temperature T. Then, we show that the fitting values of ℓ in [L] and [S] are described by the universal functions similar to Eqs. (36) and (37). For fragile liquids we take the binary mixtures $A_{80}B_{20}$ with the Stillinger–Weber potential [53] and Al_2O_3 with the Born–Meyer potential [54]. For strong liquids we take SiO_2 with the Beest–Kramer–Santen (BKS) potential [55] and also SiO_2 with the Nakano–Vashishta (NV) potential [56]. The detailed information about those simulations is found in Refs. [44–46].

The mean-square displacement $M_2(t)$ for an arbitrary particle in binary systems is calculated by using $M_2(t) = N^{-1}\sum_{j=1}^{N}\langle|\boldsymbol{X}_j(t) - \boldsymbol{X}_j(0)|^2\rangle$, where N is the total number of particles. Similarly to the hard-sphere systems, the simulation results are analyzed by using the mean-field solution given by Eq. (25) consistently. Thus, the temperature dependence of the displacement ℓ is found for each system. Because of the universality, we have $\ell q_m = L(T_c/T)$. In order to find the liquid line ℓ_l and the supercooled line ℓ_s, therefore, it is convenient to first replace $\phi(\delta)/\phi_c(\delta)$ in Eqs. (36) and (37) by T_c/T and then to fix the prefactors appeared in those lines from the fitting with the simulation results on the SW binary mixture $A_{80}B_{20}$ and SiO_2 with the NV potential. Thus, one can find the following universal functions for fragile liquids and strong liquids:

$$\ell_l(T)q_m = A_l\left[B_l\,(T_c/T)^{-1/3} - 1\right], \tag{38}$$

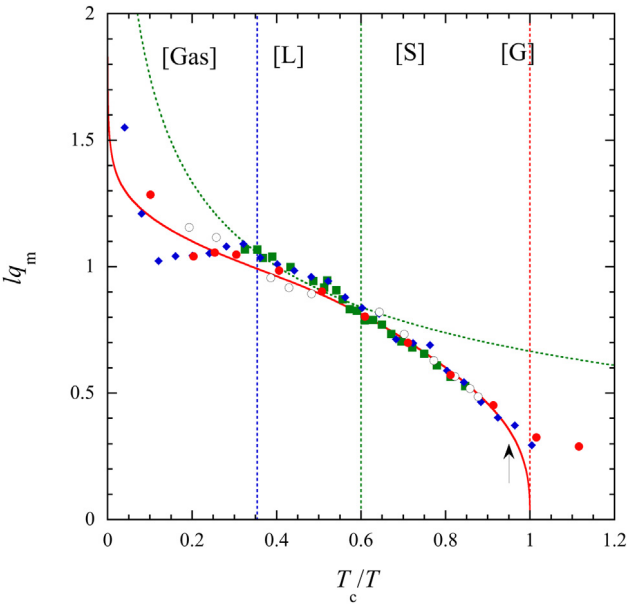

Fig. 8. (Color online) A scaled mean-displacement ℓq_m versus scaled inverse temperature T_c/T for fragile liquids. The symbols (□) indicate the length ℓ obtained from the simulations on Al_2O_3 [45,46], where $q_m = 2.7$ (Å) and $T_c \simeq 1947.8$ (K), (•) from the simulations on the SW binary mixture $A_{80}B_{20}$ [44–46], where $q_m\sigma = 7.25$ and $T_c \simeq 0.500$, (◊) from the simulations on the LJ binary mixtures $A_{80}B_{20}$ [47,48], where $q_m\sigma = 7.25$ and $T_c \simeq 0.402$, and (⊙) from the simulations on the LJ Brown binary mixtures $A_{80}B_{20}$ [57], where $q_m\sigma = 7.25$ and $T_c \simeq 0.386$. The dotted line indicates the liquid line given by Eq. (38) and the solid line the supercooled line given by Eq. (39). The vertical dotted lines indicate the scaled liquid point T_c/T_l, the scale supercooled point T_c/T_s, and the critical point $T_c/T = 1$ from left to right. The arrow indicates the glass transition point T_c/T_g.

$$\ell_s(T)q_m = \frac{1}{A_s[B_s\tilde{D}(T_c/T)^{-\mu/2} - 1]}, \tag{39}$$

where the prefactors A_i and B_i are listed in Table 2. As discussed in Refs. [34,35], the power exponent of $\tilde{D}$ depends on the systems. In fact, near the critical point we have $\tilde{D}(T_c/T) \propto (1 - T_c/T)^{10/3}$ for fragile liquids and $\tilde{D}(T_c/T) \propto (1 - T_c/T)^{11/3}$ for strong liquids, while Eq. (31) holds for hard-sphere fluids. Thus, we obtain $\ell_s(T) \propto \tilde{D}^{\mu/2} \propto (1 - T_c/T)^{1/3}$ for both types of liquids, while $\ell_s(\phi(\delta)) \propto (1 - \phi(\delta)/\phi_c(\delta))^{0.2}$ for hard-sphere fluids.

In Fig. 8, the scaled mean-displacement ℓq_m is plotted versus scaled inverse temperature T_c/T for two different fragile systems, $A_{80}B_{20}$ and Al_2O_3. In a liquid state [L] for $T_l \geq T \geq T_s$ the simulation results are described by the liquid line given by Eq. (38) well within error, while in a supercooled state [S] for $T_s \geq T \geq T_g$ they also obey the supercooled line given by Eq. (39) well within error. Here T_l is a liquid temperature, T_s a supercooled temperature, and $T_g(> T_c)$ a glass transition temperature, where $T_c/T_l \simeq 0.354$, $T_c/T_s \simeq 0.600$, and $T_c/T_g \simeq 0.949$. For comparison, the displacement obtained from the simulations on the LJ binary mixtures $A_{80}B_{20}$ [47,48] and the LJ Brown binary mixtures [57] are also plotted. They are shown to be described by Eqs. (38) and (39) within error. As discussed in Ref. [33], however, we note here that in [L] there exists a difference between a mean-displacement in molecular systems and that in suspensions. This is mainly because the short-time dynamics is governed by a ballistic motion in molecular systems, while it is done by a diffusion in suspensions. Hence the values of the prefactors A_ℓ and B_ℓ are different in both systems. On the other hand, in [S] both results obey Eq. (39) well within error. This is because the dynamics at β stage is governed by the same caging mechanism in both systems. In Fig. 9, the scaled mean-displacement ℓq_m is also plotted versus scaled inverse temperature T_c/T for SiO_2 with two different potentials, the BKS potential and the NV potential. In a liquid state [L] both results are well described by the liquid line given by Eq. (38) up to T_c/T_s within error, while in a supercooled state [S] they obey the supercooled line given by Eq. (39) well up to T_c/T_g within error, where $T_c/T_s \simeq 0.645$ and $T_c/T_g \simeq 0.848$.

4. A length cutoff

In this section, we discuss the control parameter λ dependence of cutoff b, which is obtained by solving the TMCT equation numerically. Then, we explore how it is related to the characteristic length $\ell(\lambda)$.

In order to solve the TMCT equation, one needs the static structure factor $S(q)$. In most glass-forming liquids, however, the wavevector dependence of $S(q)$ is given only numerically. Hence the numerical calculation of the TMCT equation is not easy to do in general. On the other hand, for monodisperse hard spheres, the analytic form of $S(q)$ is given by the Percus–Yevick model [36]. Thus, one can easily find the critical cutoff b_c [37,38] and also the cutoff b [31]. In this paper, therefore, we

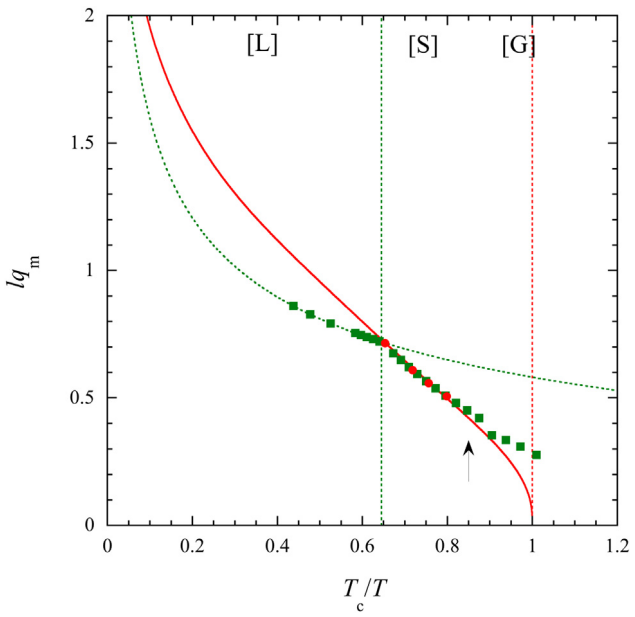

Fig. 9. (Color online) A scaled mean-displacement ℓq_m versus scaled inverse temperature T_c/T for strong liquids. The symbols (□) indicate the length ℓ obtained from the simulations on SiO_2 [45,46] with the NV potential [56], where $q_m = 1.55$ (Å) and $T_c \simeq 2544.2$ (K), and (•) from the simulations on SiO_2 [45,46] with the BKS potential [55], where $q_m = 1.55$ (Å) and $T_c \simeq 2876.1$ (K). The dotted line indicates the liquid line given by Eq. (38) and the solid line the supercooled line given by Eq. (39). The details are the same as in Fig. 8.

focus only on the monodisperse hard spheres. However, we should mention here that if $S(q)$ is known for the other systems, exactly the same approach as that employed here is directly applicable to them.

We first discuss the critical point $\phi_c(0)$. By solving Eq. (15), one can first obtain the critical volume fraction $\phi_c(0) \simeq 0.5817$ for $b \le b_c$, where the maximum critical cutoff b_c is given by $\sigma/b_c = 27$. We note here that in the previous paper [37] the same critical value $\phi_c(0)$ has been found at $\sigma/b = 40$. As mentioned before, this result is reasonable because the critical value does not change for $b \le b_c$. Next, we solve the TMCT equation given by Eq. (10) numerically for $\phi < \phi_c$. Here we note that the TMCT equation contains two unknown parameters, the damping constant γ and the cutoff b. Firstly, the parameter γ is fixed as follow. Since the nonlinear term in Eq. (18) is neglected for a short time of order τ_γ, $M_2(t)$ obeys

$$M_2(t) \simeq 6v_{th}^2(\gamma t - 1 + e^{-\gamma t})/\gamma^2. \tag{40}$$

Hence the value of γ is found so that Eq. (40) coincides with the simulation results at least up to a time scale of order τ_f, where $\tau_\gamma < \tau_f$. Secondly, the cutoff b is fixed so that the long-time self-diffusion coefficient D_s^L given by Eq. (20) coincides with the simulation results.

In the MD simulations on monodisperse hard spheres, however, there is no diffusion data available in a supercooled state for $\phi \ge \phi_s$ because the crystallization occurs. On the other hand, the numerical solutions obtained by using the PY static structure factor do not show any crystallization. Hence one can in principle find any numerical solutions up to the critical point ϕ_c. In order to obtain the simulation results for higher volume fractions, we use the universality discussed in Section 2.3. In fact, by using Eq. (32), one can shift the simulation results obtained for polydisperse hard spheres ($\delta \ne 0$) to those for monodisperse ones. In Figs. 10 and 11, the damping constant γ and the displacement ℓ obtained for a wide range of ϕ by employing such a universality are plotted versus $\phi(0)$ in a monodisperse unit, respectively. As ϕ increases, γ increases monotonically up to $\phi_g(0)(\simeq 0.580)$. By using such fitting values of γ and the simulation results for D_s^L, one can in principle solve the TMCT equation (10) with the PY static structure factor numerically. However, it is technically hard to solve it even numerically because of the double integrals in the memory term. Therefore, we start from the following original TMCT equation instead [28–31]:

$$\frac{\partial^2 K_\alpha(q,t)}{\partial t^2} = \frac{q^2 v_{th}^2}{S_\alpha(q)} - \gamma \frac{\partial K_\alpha(q,t)}{\partial t} - \int_0^t ds \Delta\varphi_\alpha(q, t-s) \frac{\partial}{\partial s} K_\alpha(q,s). \tag{41}$$

As shown in Ref. [31], Eq. (41) is easily obtained by making an approximation (A2) given by $f_\alpha(q,\tau)/f_\alpha(q,s) = 1$ in Eq. (10). Here we note that the critical point obtained by Eq. (41) is the same as that obtained by Eq. (10) [31]. One can now solve Eq. (41) numerically under the fixed values of γ and D_s^L. In Fig. 12, the inverse scaled length cutoff $(bq_m)^{-1}$ is thus plotted versus ϕ in a monodisperse unit. Here the cutoff $b(\phi)$ is obtained by using the simulation results for $\phi < \phi_g$ and is shown to decrease as ϕ increases. For $\phi \ge \phi_g$, however, the TMCT equation cannot be used to find $b(\phi)$ since the system is out of

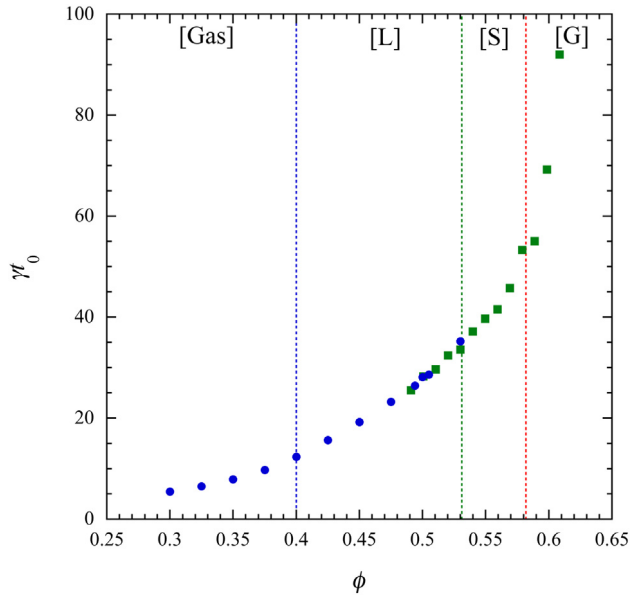

Fig. 10. (Color online) A scaled damping constant γt_0 versus volume fraction ϕ in a monodisperse unit. The symbols (•) indicate the fitting values obtained from the simulation results for monodisperse hard spheres. The symbols (□) indicate the fitting values obtained from the simulation results for polydisperse hard spheres at $\delta = 0.15$, where the volume fraction $\phi(\delta = 0.15)$ is shifted to $\phi(0)$ by using Eq. (32). The details are the same as in Fig. 6.

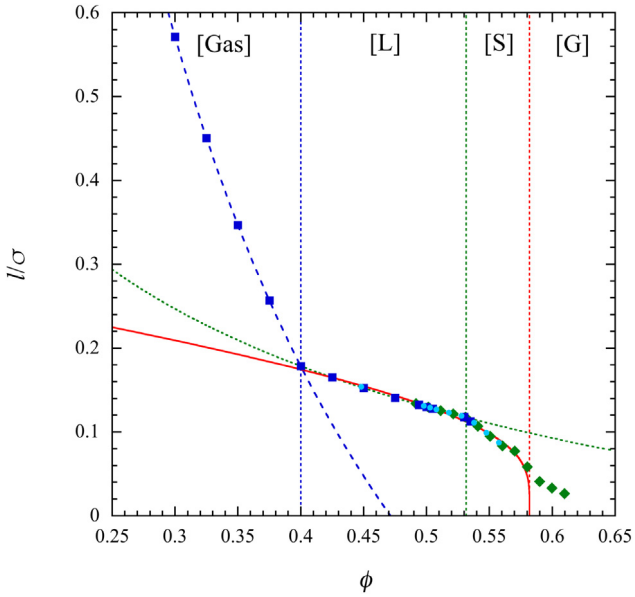

Fig. 11. (Color online) A scaled characteristic length ℓ/σ versus volume fraction ϕ in a monodisperse unit. The symbols (□), (○), and (◇) indicate the fitting values obtained from the simulation results at $\delta = 0.0$, 0.06, and 0.15, respectively, where the volume fraction $\phi(\delta)$ is shifted to $\phi(0)$ by using Eq. (32). The details are the same as in Fig. 7.

equilibrium. We should note here that the maximum critical cutoff b_c is found directly from Eq. (15) independently of the simulation results, leading to $\sigma/b_c = 27$ and $(b_c q_m)^{-1} = 3.6726$, where $q_m\sigma = 7.3518$ at $\phi = \phi_c(0)$. In a supercooled state [S], the cutoff b is thus shown to satisfy $q_m^{-1} > \ell \geq b \geq b_c$.

Finally, we check how b is physically related to ℓ, although it satisfies the inequality $\ell \geq b$ in [S]. As discussed in Ref. [31], the approximation (A2) made in Eq. (10) to obtain Eq. (41) causes a discrepancy between the simulation results and the numerical solutions. In Fig. 13, such a discrepancy is clearly seen for $M_2(t)$ with $\delta = 0.15$ at β stage in [S]. The deviation of the TMCT solutions from the simulation results at β stage becomes larger and larger as $\phi(0.15)$ increases from 0.510, while for $\phi(0.15) \leq 0.510$ there is no deviation since the memory term is negligibly small [31]. One can use Eq. (25) for the

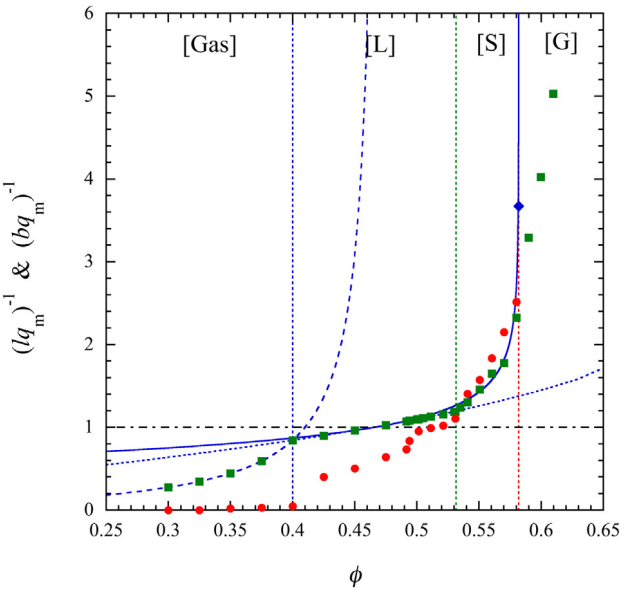

Fig. 12. (Color online) A inverse scaled length cutoff $(bq_m)^{-1}$ and an inverse scaled displacement $(\ell q_m)^{-1}$ versus scaled volume fraction $\phi/\phi_c(0)$ in a monodisperse unit. The symbols (●) indicate the inverse scaled cutoff $(bq_m)^{-1}$ obtained by solving the TMCT equation with the PY static structure factor and (◇) the inverse scaled maximum critical cutoff $(b_c q_m)^{-1}(= 3.6726)$. The symbols (□) indicate the inverse scaled length $(\ell q_m)^{-1}$ obtained from the simulations on hard spheres at $\delta = 0$, 0.06, and 0.15. The dashed line indicates the gas line $(\ell_f q_m)^{-1}$ given by Eq. (33), the dotted line the liquid line $(\ell_l q_m)^{-1}$ given by Eq. (34), and the solid line the supercooled line $(\ell_s q_m)^{-1}$ given by Eq. (37). The horizontal dot-dashed line indicates the first peak position $bq_m = 1$ of the PY static structure factor $S(q)$. The details are the same as in Fig. 11.

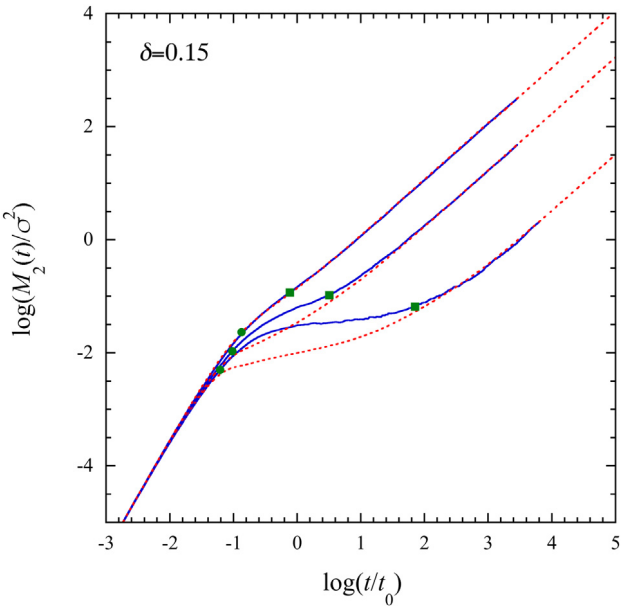

Fig. 13. (Color online) A log–log plot of the scaled mean-square displacement $M_2(t)/\sigma^2$ versus scaled time t/t_0 for hard-sphere fluids with $\delta = 0.15$ at $\phi = 0.510$ [L], 0.560 [S], and 0.590 [S] from left to right. The solid lines indicate the simulation results for $M_2(t)$ and the dotted lines for the TMCT solutions. The symbols (●) indicate the mean-free time τ_f and (□) the β-relaxation time τ_β.

TMCT solutions to find the displacement ℓ_{TMCT} in [S]. Then, it is shown that ℓ_{TMCT} is always smaller than ℓ and coincides with b within error. Thus, it turns out that a small difference between ℓ and b in [S] results from the approximation (A2). This means that if one can solve Eq. (10) itself, such a difference may disappear, leading to $b = \ell$. Similarly to Eq. (37), one can

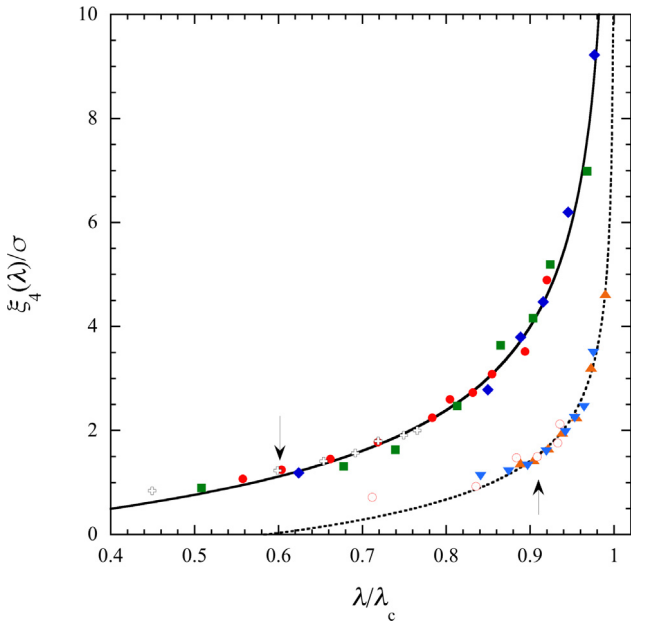

Fig. 14. (Color online) A plot of the scaled length ξ_4/σ versus scaled control parameter λ/λ_c. The symbols indicate the simulation results on ($\diamond$) the LJ binary mixture [21] with $T_c \simeq 0.570$, ($\square$) the LJ binary mixture [22] with $T_c \simeq 0.406$, ($\circ$) the Wahnström mixture [23] with $T_c \simeq 0.555$, ($+$) the LJ binary mixture [24] with $T_c \simeq 0.359$, ($\triangledown$) the Kob–Andersen lattice glass model [25] with $\phi_c \simeq 0.467$, and ($\triangle$) the polydisperse hard spheres of $N = 1372$ [26] with $\phi_c \simeq 0.5853$. The symbols ($\odot$) indicate the experimental results for all particles of binary colloids [27] with $\phi_c \simeq 0.5819$. Here $\ell_0 = \sigma$, except that $\ell_0 = \sigma/2$ in [22]. The solid line indicates the supercooled line given by Eq. (43) with $A_4 \simeq 3.7888$ and $B_4 \simeq 0.9538$ and the dotted line with $A_4 \simeq 4.2939$ and $B_4 \simeq 0.8386$, where the asymptotic forms $\tilde{D}(T_c/T) = (1 - T_c/T)^{10/3}$ and $\tilde{D}(\phi/\phi_c) = (1 - \phi/\phi_c)^2$ in [S] have been used to obtain Eq. (43). The arrows indicate the supercooled point; ($\downarrow$) $T_c/T_s \simeq 0.6$ and ($\uparrow$) $\phi_s/\phi_c \simeq 0.913$.

also show that b obeys the same power law as that for ℓ_s and finds

$$b(\phi(\delta))q_m(\delta) = \frac{1}{A_b[B_b\tilde{D}(\phi(\delta))^{-\mu/2} - 1]}, \tag{42}$$

where $A_b \simeq 0.2872$ and $B_b \simeq 4.6341$. Near the critical point, therefore, we obtain $b(\phi) \propto \tilde{D}^{\mu/2} \propto \ell_s(\phi)$. Thus, we conclude that b in [S] must be physically identical to ℓ itself. On the other hand, in [Gas] and [L] we have $b > \ell$. Hence b is independent of the characteristic lengths in both states and just plays a role in adjusting a magnitude of nonlinear memory term so that the calculated diffusion coefficient coincides with that of the simulations. The nonlinear memory term is thus shown to play a crucial role only in [S] but not in [Gas] and [L]. We note here that the similar situation has been already discussed for two types of glass-forming materials based on the simplified TMCT equation [29,30].

5. Summary

In this paper, we have focused only on the characteristic length at β stage. We have proposed a systematic method how to find a reasonable value of the cutoff $b(\lambda)$ contained in the nonlinear memory function of TMCT equation. As a simple example, the TMCT equation has been calculated numerically by using the PY static structure factor, where the cutoff b is set so that the calculated long-time self-diffusion coefficient D_s^L coincides with that obtained from the simulation results for hard spheres. Thus, the volume fraction dependence of b has been obtained consistently. In order to clarify the physical meaning of $b(\phi)$, the mean displacement $\ell(\phi)$ in the β-relaxation stage has been also introduced based on the mean-field theory, independently of b. Both in a gas and a liquid states $\ell(\phi)$ has been shown to be a characteristic length since it is related to the mean-free path and the inter-particle distance, respectively. In those states, however, $b(\phi)$ has been shown to be physically independent of $\ell(\phi)$. On the other hand, in a supercooled state $\ell(\phi)$ and $b(\phi)$ have been shown to obey the same power-law form. Thus, it has been concluded that b is physically identical to the characteristic length ℓ itself at β stage.

Finally, we briefly mention the power-law form of the correlation length ξ_4 for dynamic heterogeneity at α stage in [S] and compare it with that of ℓ_s at β stage. The four-point dynamic correlation length $\xi_4(\lambda)$ has been numerically obtained from the simulations [21–26]. Analyzing those numerical results by using Eqs. (30) and (39), one can then obtain

$$\xi_4(\lambda) = A_4\left[B_4\tilde{D}(\lambda/\lambda_c)^{-\mu/2} - 1\right]\ell_0, \tag{43}$$

where A_4 and B_4 are fitting parameters to be determined and ℓ_0 an adjustable length unit. In Fig. 14, the simulation results for ξ_4 are plotted versus scaled control parameter λ/λ_c together with Eq. (43). Those results are thus shown to be well described

by Eq. (43) within error. For comparison, the experimental results for $\xi_4(\phi)$ on binary colloids [27] are also plotted in Fig. 14. They are also shown to obey Eq. (43) within error. Since $\xi_4 \propto \tilde{D}^{-\mu/2}$ near the critical point, from Eqs. (39) and (43) one can find an interesting relationship between ℓ_s and ξ_4 as

$$\xi_4(\lambda) \propto \ell_s(\lambda)^{-1} \propto \tilde{D}^{-\mu/2}. \tag{44}$$

This relation may suggest that as time goes on from β stage to α stage in [S], the cooperative phenomena between many shrinking cages start to play an important role in causing dynamic heterogeneity. In fact, such a gathering of cages has been discussed in the previous papers [11–15]. Using Eqs. (30) and (44), one can then write τ_α as

$$\tau_\alpha(\lambda) \propto \xi_4(\lambda)^2/\tilde{D}(\lambda/\lambda_c). \tag{45}$$

This expression is in general expected to hold for the self-diffusion process of any glass-forming materials. This will be discussed elsewhere together with a derivation of a TMCT equation for a new relevant variable with a new cutoff at α stage.

References

[1] U. Bengtzelius, W. Götze, A. Sjölander, J. Phys. C 17 (1984) 5915;
E. Leutheusser, Phys. Rev. A 29 (1984) 2765.
[2] W. Götze, in: J.P. Hansen, D. Levesque, J. Zinn-Justen (Eds.), Liquids, Freezing and Glass Transition, North-Holland, Amsterdam, 1991.
[3] C.A. Angell, K.L. Ngai, G.B. McKenna, P.F. McMillan, S.W. Martin, J. Appl. Phys. 88 (2000) 3113.
[4] P.G. Debenedetti, F.H. Stillinger, Nature 410 (2001) 259.
[5] M. Tokuyama, I. Oppenheim (Eds.), Proceedings of the Third International Symposium on Slow Dynamics in Complex Systems, in: CP **708**, AIP, New York, 2004, Proceedings of the Fourth International Symposium on Slow Dynamics in Complex Systems, CP **1518**, AIP, New York 2013.
[6] K. Binder, W. Kob, Glassy Materials and Disordered Solids, World Scientific, Singapore, 2005.
[7] A. Heuer, J. Phys.: Cindens. Matter 20 (2008) 373101.
[8] G. Parisi, F. Zamponi, Rev. Modern Phys. 82 (2010) 789.
[9] L. Berthier, G. Biroli, Rev. Modern Phys. 83 (2011) 587.
[10] G. Biroli, J.P. Garrahan, J. Chem. Phys. 138 (2013) 12A301.
[11] M.M. Hurley, P. Harrowell, Phys. Rev. E 52 (1995) 1694.
[12] M. Tokuyama, Y. Enomoto, I. Oppenheim, Phys. Rev. E 56 (1997) 2302.
[13] M. Tokuyama, Y. Enomoto, I. Oppenheim, Physica A 270 (1999) 380.
[14] R. Yamamoto, A. Onuki, Phys. Rev. E 58 (1998) 3515.
[15] B. Doliwa, A. Heuer, Phys. Rev. E 61 (2000) 6898.
[16] H. Sillescu, J. Non-Cryst. Solids 243 (1999) 81.
[17] M.D. Ediger, Annu. Rev. Phys. Chem. 51 (2000) 99.
[18] S. Franz, G. Parisi, J. Phys.: Condens. Matter 12 (2000) 6335.
[19] B.M. Erwin, R.H. Colby, J. Non-Cryst. Solids 307–310 (2002) 225.
[20] S. Karmakar, C. Dasgupta, S. Sastry, Proc. Natl. Acad. Sci. USA 106 (2009) 3675.
[21] N. Lacevic, F. Starr, T.B. Schroder, S.C. Glotzer, J. Chem. Phys. 119 (2003) 7372.
[22] L. Berthier, Phys. Rev. E 69 (2004) 020201;
S. Whitelam, L. Berthier, J.P. Garrahan, Phys. Rev. Lett. 92 (2004) 185705.
[23] A. Malins, J. Eggers, P. Royall, S.R. Williams, H. Tanaka, J. Chem. Phys. 138 (2013) 12A535.
[24] H.L. Peng, Th. Voigtmann, Phys. Rev. E 94 (2016) 042612.
[25] R. Pastore, M.P. Ciamarra, A. de Candia, A. Coniglio, Phys. Rev. Lett. 107 (2011) 065703.
[26] A.J. Dunleavy, K. Wiesner, R. Yamamoto, C.P. Royall1, Nature Commun. 6 (2015) 1.
[27] T. Narumi, S.V. Franklin, K.W. Desmond, M. Tokuyama, E.R. Weeks, Soft Matter 7 (2011) 1472.
[28] M. Tokuyama, Physica A 395 (2014) 31.
[29] M. Tokuyama, Physica A 430 (2015) 156.
[30] M. Tokuyama, Physica A. 465 (2017) 229.
[31] M. Tokuyama, Physica A 484 (2017) 453.
[32] M. Tokuyama, Physica A 364 (2006) 23.
[33] M. Tokuyama, Physica A 378 (2007) 157.
[34] M. Tokuyama, J. Phys. Chem. B 115 (2011) 14030.
[35] M. Tokuyama, AIP CP 1518 (2013) 47.
[36] J.K. Percus, G.J. Yevick, Phys. Rev. 110 (1958) 1.
[37] Y. Kimura, M. Tokuyama, IL Nuovo Cimento C 39 (2016) 300.
[38] T. Narumi, M. Tokuyama, Phys. Rev. E 95 (2017) 032601.
[39] H. Mori, Progr. Theoret. Phys. 33 (1965) 423.
[40] M. Tokuyama, H. Mori, Progr. Theoret. Phys. 54 (1975) 918.
[41] M. Tokuyama, H. Mori, Progr. Theoret. Phys. 55 (1976) 411.
[42] R. Kubo, J. Phys. Soc. Japan 17 (1962) 1100.
[43] A. Rahman, K.S. Singwi, A. Sjölander, Phys. Rev. 126 (1962) 986.
[44] M. Tokuyama, S. Enda, Physica A 392 (2013) 2999.
[45] S. Enda, M. Tokuyama, AIP CP 1518 (2013) 324.
[46] M. Tokuyama, S. Enda, J. Kawamura, Physica A 442 (2016) 1.
[47] W. Kob, H.C. Andersen, Phys. Rev. Lett. 73 (1994) 1376.
[48] T. Narumi, M. Tokuyama, Phys. Rev. E 84 (2011) 022501.
[49] M. Tokuyama, H. Yamazaki, Y. Terada, Phys. Rev. E 67 (2003) 062403.
[50] M. Tokuyama, H. Yamazaki, Y. Terada, Physica A 328 (2003) 367.
[51] M. Tokuyama, Y. Terada, J. Chem. Phys. B 109 (2005) 21357.
[52] M. Tokuyama, T. Narumi, E. Kohira, Physica A 385 (2007) 439.
[53] T.A. Weber, F.H. Stillinger, Phys. Rev. B 31 (1985) 1954.
[54] V.V. Hoang, Phys. Rev. B 70 (2004) 134204.
[55] B.W.H. van Beest, G.J. Kramer, R.A. van Santen, Phys. Rev. Lett. 64 (1990) 1955.
[56] A. Nakano, L.S. Bi, R.K. Kalia, P. Vashishta, Phys. Rev. B 49 (1994) 9441.
[57] E. Flenner, G. Szamel, Phys. Rev. E 72 (2005) 031508.